Icarus 281 (2017) 90–102

Contents lists available at ScienceDirect

Icarus

journal homepage: www.elsevier.com/locate/icarus

Coupled orbital-thermal evolution of the early Earth-Moon system with a fast-spinning Earth

ZhenLiang Tian[a,*], Jack Wisdom[a], Linda Elkins-Tanton[b]

[a] Massachusetts Institute of Technology, Cambridge, MA 02139, USA
[b] School of Earth and Space Exploration, Arizona State University, Tempe, AZ 85281, USA

ARTICLE INFO

Article history:
Available online 6 September 2016

Keywords:
Moon
Planetary dynamics
Thermal histories
Solid body tides

ABSTRACT

Several new scenarios of the Moon-forming giant impact have been proposed to reconcile the giant impact theory with the recent recognition of the volatile and refractory isotopic similarities between Moon and Earth. Two scenarios leave the post-impact Earth spinning much faster than what is inferred from the present Earth-Moon system's angular momentum. The evection resonance has been proposed to drain the excess angular momentum, but the lunar orbit stays at high orbital eccentricities for long periods in the resonance, which would cause large tidal heating in the Moon. A limit cycle related to the evection resonance has also been suggested as an alternative mechanism to reduce the angular momentum, which keeps the lunar orbit at much lower eccentricities, and operates in a wider range of parameters. In this study we use a coupled thermal-orbital model to determine the effect of the change of the Moon's thermal state on the Earth-Moon system's dynamical history. The evection resonance no longer drains angular momentum from the Earth-Moon system since the system rapidly exits the resonance. Whereas the limit cycle works robustly to drain as much angular momentum as in the non-thermally-coupled model, though the Moon's tidal properties change throughout the evolution.

1. Introduction

The giant impact theory for lunar formation (Hartman and Davis, 1975; Cameron and Ward, 1976) can account for the large angular momentum of the Earth-Moon system, the late formation of the Moon, the Moon's deficiency of iron and volatiles, and the presence of a magma ocean in the early lunar history. Simulations of the impact and accretion processes led to a well accepted standard model of lunar formation (Canup and Asphaug, 2001; Canup, 2004, 2008), in which a Mars-sized body collided with the proto-Earth, forming an Earth-Moon system with the angular momentum equal to the present value. This model fit well with multiple lines of observations, until the relatively recent recognition of the isotopic similarities of the elements oxygen (Wiechert et al., 2001), potassium (Huang et al., 2016), chromium (Lugmair and Shukolyukov, 1998), tungsten (Touboul et al., 2007) and titanium (Zhang et al., 2012) between lunar samples and the terrestrial mantle. These isotopic similarities, especially of highly refractory elements like Ti, which is not likely to have equilibrated during a post-impact equilibration phase (Pahlevan and Stevenson, 2007), are evidence that the lunar material was predominantly derived from the proto-Earth, unless the impacting planet had isotopic signatures very close to those of the proto-Earth (Mastrobuono-Battisti et al, 2015; Kaib and Cowan, 2015). However, the standard model indicates that the Moon should have mostly been derived from the impactor, given the dynamical constraint that the angular momentum of the Earth-Moon system at the time of lunar formation should be close to the present value.

Several new impact scenarios (Cuk and Stewart, 2012; Canup, 2012; Reufer et al., 2012) have been proposed to reconcile this contradiction. While these models can produce a Moon with essentially the same materials that make up the terrestrial mantle, they all assume impact angular momenta much higher than the current angular momentum of the Earth-Moon system. The Reufer et al. scenario assumes that the excess angular momentum is removed through the escape of a portion of the impactor mass from the system just after the impact. The other two assume an Earth-Moon system with an initial angular momentum much higher than the current value. With dynamical simulations that begin with a fast-spinning Earth, it was suggested (Cuk and Stewart, 2012) that the excess angular momentum can be transferred to the Earth's orbit around the Sun through an orbital resonance between the precession of the lunar pericenter and the Earth's orbit around the Sun. Upon the system's entry into this resonance, called the

* Corresponding author.
E-mail addresses: zlt@mit.edu (Z. Tian), wisdom@mit.edu (J. Wisdom).

http://dx.doi.org/10.1016/j.icarus.2016.08.030
0019-1035/

evection resonance, the period of precession of the lunar pericenter is locked to one year, the angle between the direction of the lunar pericenter and the direction of the Sun from the Earth (the evection angle) begins to oscillate about either $\pi/2$ rad or $3\pi/2$ rad, and the eccentricity of the lunar orbit is raised. While the system is captured in the evection resonance, the eccentricity is maintained at a high value, the semi-major axis of the lunar orbit decreases, and the Earth despins, all contributing to the loss of angular momentum from the Earth-Moon system. With this orbital mechanism to remove the excess angular momentum, the two giant impact scenarios work well to produce an Earth-Moon system that could meet both the chemical and angular momentum constraints.

However, passage through the evection resonance would cause large tidal heating in the Moon. To illustrate the problem, consider the heating in the Moon with fixed parameters. The resonance excites the eccentricity of the lunar orbit to as high as 0.5, and keeps the system trapped in it for a period of ~100,000 years, when the Moon is just about 4–7 Earth radii (R_e) from the Earth. Take the rate of tidal heating of the Moon to be $\frac{21}{2}\frac{Gm_E{}^2e^2R_M{}^5n}{a^6}\frac{k_2}{Q}$ (Peale and Cassen, 1978), where G, m_E, R_M, e, n, a, k_2, Q are the gravitational constant, mass of the Earth, radius of the Moon, the lunar orbit's eccentricity, mean motion, semi-major axis, degree-2 potential Love number, and dissipation factor of the Moon. Approximate k_2 with $\frac{3\rho gR_M}{19\mu}$, where μ, ρ, g are the Moon's rigidity, density and surface acceleration. Taking the time spent in the resonance to be 100,000 years, e = 0.5, Q = 100, $\rho = 3.34\times10^3$ kg m^{-3}, $\mu = 6.5\times10^{10}$ N m^{-2}, $g = 1.62$ m s^{-2}, the Earth-Moon distance to be 6.5 Earth radii, the Moon's specific heat capacity to be 1256 J kg^{-1}C^{-1}, and the lunar mass to be 7.438×10^{22} kg, the temperature of the Moon will be raised by ~10,000 °C after the system's passage through the evection resonance. Such an increase in temperature would have completely vaporized the Moon! So the assumption of fixed parameters is inadequate. It is necessary to take into account how the large tidal heating in the Moon changes the parameters and consequently the dynamical evolution.

With new orbital simulations that use a more complete tidal model, and are run over a greater range of parameters, an alternative mechanism was found to be capable of removing the Earth-Moon system's angular momentum while avoiding the drawbacks of the evection resonance (Wisdom and Tian, 2015). In this mechanism, which is a limit cycle related to the evection resonance, the lunar eccentricity oscillates in a range with an upper bound typically near 0.1, and the evection angle circulates from 0 to 2π rad with the same period as the oscillation of eccentricity. During the system's capture in the limit cycle, the semi-major axis of the lunar orbit decreases, and the Earth despins, so the angular momentum of the Earth-Moon system is also reduced, as in the evection resonance. Compared with the evection resonance, this mechanism excites the system to orbital eccentricities smaller by a factor of 3–5, even using the upper bound of eccentricity oscillation. Since the rate of tidal heating is proportional to the square of eccentricity, the Moon is therefore much less seriously heated by tides through the limit cycle. The limit cycle has an additional and significant advantage that it occurs over a much wider range of tidal parameter than the evection resonance.

How well do these two mechanisms (the evection resonance and the evection limit cycle) work when considering the consequences of tidal heating? Heating of a body must induce changes in the body's tidal properties, and thus affect the orbital evolution by changing the tidal accelerations. The purpose of this study is to determine the manner and extent of the effect of the thermal evolution of the Moon on the orbital evolution that starts with a fast-spinning Earth, and to evaluate the effectiveness of the limit cycle and the evection resonance in removing the Earth-Moon system's excess angular momentum.

2. Model

The computational scheme is composed of two interacting subsystems, the thermal evolution of the Moon and the orbital evolution of the Earth, Moon, and Sun. The thermal system tracks the changes of the Moon's thermal profile, structure, and tidal properties over time. The orbital system tracks the locations and velocities of the Earth, Moon, and Sun, as well as the Earth and Moon's rotational state.

At every time step, the thermal system reads the values of lunar orbital eccentricity and semi-major axis from the orbital system, because they are needed to calculate the heating of the Moon. The thermal system determines the values of the Moon's tidal potential Love number, k_2, and dissipation factor, Q, which are then used by the orbital system for calculating the tidal accelerations.

In the thermal model, we begin with a lunar structure that is suggested by magma ocean solidification studies: a thin (5 km), solid anorthositic flotation lid overlies a liquid magma ocean of ~100 km in depth, which overlies a solid interior. According to some solidification models (for example, Elkins–Tanton et al., 2011), an original magma ocean as deep as 1000 km, without a lid on the surface, can solidify 80% in just several thousand years, as heat efficiently escapes the magma ocean to space by radiation. After this point, plagioclase begins to crystalize and buoyantly segregates from the magma to form a lid at the surface. The presence of the lid switches the heat loss regime from radiation from a free liquid surface to the significantly less efficient thermal conduction through the solid lid. Then it takes tens of millions of years (My) to solidify the remaining magma. During the first several thousand years, tidal dissipation in the Earth dominates the orbital evolution of the Earth-Moon system, since the dissipation in the Moon without a solid lid overlying the magma ocean would be very small. The orbital change is mainly an increase in the lunar orbit's semi-major axis, with little change in eccentricity and the system's angular momentum. Since several thousand years is short compared to the ~100,000 years the system spends in the evection resonance or limit cycle, and nothing significant happens during this period, we choose to start the evolution assuming 80% of the magma ocean has already solidified and that a thin plagioclase lid has been formed.

For radiogenic heating in the Moon, we assume that all the heat-generating isotopes are retained in the magma during magma ocean solidification. We infer the amount of heating according to chondritic abundances of radiogenic isotopes, assuming the simulated evolution begins 60 My after the formation of calcium-aluminum-rich inclusions, as suggested by tungsten isotope chronologies (Touboul et al., 2007). We find that radiogenic heating is not a significant contribution to the energy budget.

The orbital system's set-up and evolution are the same as in Wisdom and Tian (2015), and we briefly outline it here. We evolve the locations and velocities of the Earth, Moon, and Sun using the N-body symplectic mapping method (Wisdom and Holman, 1991). We also evolve the rigid body rotational states of the Earth and Moon, and include the spin-orbit interactions of the Earth with the lunar orbit and the Earth's orbit around the Sun, and the Moon's spin-orbit interactions with the lunar orbit around the Earth. In Wisdom and Tian (2015) we used both the quaternion equations of motion (Sussman and Wisdom, 2015) and the Lie-Poisson algorithm (Touma and Wisdom, 1993) for the rigid body dynamics, and the two approaches produced the same results. In this study we use the Lie-Poisson integrator.

The full form of the Darwin–Kaula tide (Kaula 1964) is used for computing the tidal accelerations of the Earth and Moon. The tidal potential is expanded to a sum of terms of different frequencies. Each frequency component of the tidal potential, V_{lmpq}, is specified by the combination of numbers (l,m,p,q),

as is the phase lag for each frequency, which is denoted as ε_{lmpq}. We adopt a constant-Q model (Q being frequency-independent rather than time-independent) with $\epsilon_{lmpq} = 1/Q \cdot sign(m(\dot{\Omega} - \dot{\theta}) + (l-2p)\dot{\omega} + (l-2p+q)n)$, where $\dot{\Omega}$ and $\dot{\omega}$ denote the rate of change of the perturber's longitude of ascending node and argument of pericenter, n denotes the orbital mean motion, $\dot{\theta}$ denotes the rotation rate of the deforming body. The constant Q model is consistent with what is known about the frequency dependence of the Q of the present day Moon (Williams et al., 2005, 2014). A disadvantage of the constant Q model is that the tidal phase lags exhibit discontinuities near commensurabilities, which presumably only approximate the actual behavior. An alternate choice could have been the popular Mignard tidal model (Mignard, 1979), but in this model the frequency dependence of the Q is not consistent with what is observed. We feel the advantages of the constant Q model outweigh its disadvantages.

The evolution of the thermal system is governed by a set of processes including tidal heating and thermal diffusion in the lid, partial melting and melt migration in the lid, crystallization and release of latent heat and radiogenic heating in the magma ocean, and exchange of heat between the magma ocean and the lid. We illustrate each of them below.

2.1. Tidal heating and thermal diffusion in the lid

The contribution of tidal heating and conduction of heat to the lid's temperature evolution is described by

$$\frac{\partial T}{\partial t} = \frac{2\kappa}{r}\frac{\partial T}{\partial r} + \frac{\partial}{\partial r}\left(\kappa \frac{\partial T}{\partial r}\right) + \frac{H}{\rho_l C_p}, \tag{1}$$

where T is the local temperature, r is the radius, t is the time, κ is the thermal diffusivity, ρ_l is the density, C_p is the specific heat capacity, H is the local volumetric tidal heating rate. We use $C_p = 1256\,\mathrm{J\ kg^{-1}\ ^\circ C^{-1}}$ and $\kappa = 10^{-6}\,\mathrm{m^2\ s^{-1}}$. We take $\rho_l = 2927\,\mathrm{kg\ m^{-3}}$, the average grain density of the crust (Wieczorek et al., 2013). The current actual crustal density with porosity is $2550\,\mathrm{kg\ m^{-3}}$, but the porosity is the result of billions of years of accumulative impact cratering, which was not the case for the earliest period of the Moon. We also made simulations using the current density ($2550\,\mathrm{kg\ m^{-3}}$) and find that the results are insensitive of the choice between the two densities. The first two terms on the right side constitute Fourier's law written in spherical coordinates, with the approximation that the heating and temperature are azimuthally homogeneous.

In the computation, first we parameterize the depth of each layer using y, which varies from 0 (at the surface) to 1 (at the bottom of the lid). So

$$r = R_M - \delta_l \cdot y, \tag{2}$$

where δ_l is the thicknesses of the lid. Let $T'(t, y) = T(t, r)$, and note that δ_l is varying with time, Eq. (1) becomes

$$\frac{\partial T'}{\partial t} = \left(\frac{y\dot{\delta}_l}{\delta_l} - \frac{2\kappa}{r\delta_l}\right)\frac{\partial T'}{\partial y} + \frac{\kappa}{\delta_l^2}\frac{\partial^2 T'}{\partial y^2} + \frac{H}{\rho_l C_p} \tag{3}$$

Then we discretize the lid to 100 layers of thickness $\Delta r = \delta_l\ \Delta y$ ($\Delta y = 1/100$). Denote the temperature of the ith layer to be T^i, Eq. (3) becomes

$$\frac{dT^i}{dt} = \left(\frac{y\dot{\delta}_l}{\delta_l} - \frac{2\kappa}{r\delta_l}\right)\left(\frac{T^{i+1} - T^{i-1}}{2\Delta y}\right) + \frac{\kappa}{\delta_l^2}\left(\frac{T^{i+1} - 2T^i + T^{i-1}}{\Delta y^2}\right) + \frac{H}{\rho_l C_p} \tag{4}$$

We evolve the lid temperatures according to Eq. (4). Note that this equation does not include the thermal effects of partial melting and melt migration, which is treated separately and will be elaborated later.

The expression for the azimuthally averaged rate of volumetric tidal heating in the lid is derived based on Peale and Cassen(1978), and we correct and outline it in the appendix. It is

$$H = \mu G^2 {m_E}^2 n {R_M}^2 a^{-6} Q^{-1} g^{-2} {k_2}^2 (21/5 \cdot {\alpha_0}^2 + 42/5 \cdot {\alpha_1}^2 - 252/5 \cdot \alpha_1\alpha_2 + 126{\alpha_2}^2 + 252/5 \cdot {\alpha_3}^2) \times (e^2 + 403/56e^4 + 1207/42e^6 + 336953/4032e^8 + \ldots), \tag{5}$$

where $g = 1.62\,\mathrm{m\ s^{-2}}$ is the surface acceleration, and the α_i are functions of the layer's position and the lid thickness, which are presented in the appendix. In this expression, a, Q, k_2, e and α_i all evolve over time.

The dissipation factor, Q, for a layer at temperature T is given by the Ojakangas and Stevenson (1986) formula

$$\frac{1}{Q}(T) = \frac{1}{Q_{max}} + \left[\frac{1}{Q_{min}} - \frac{1}{Q_{max}}\right]\left(\frac{T}{T_p}\right)^n, \tag{6}$$

where T_p is the melting temperature of plagioclase. We take $T_p = 1550\,^\circ\mathrm{C}$. We set $Q_{min} = 20$, and let Q_{max} vary with the runs. Experimentally, the parameter n ranges from 20 to 30 (Ojakangas and Stevenson, 1986); we use 25. The choice of $Q_{min} = 20$ is somewhat arbitrary. The current Q of the Moon is approximately 20 (Williams et al., 2005, 2014).

We take an effective $1/Q_m$ of the Moon for use in the orbital system to be the average of the $1/Q$ of the individual lid layers.

The potential Love number k_2 as a function of the lid thickness is given in the appendix. The rigidity of the shell is taken to be $\mu = 6.5 \times 10^9\,\mathrm{N\ m^{-2}}$. This is an order of magnitude smaller than the rigidity used by Peale and Cassen (1978) based on seismic velocities in today's cold Moon. We use a lower rigidity because of the high temperatures in the lid during the early epoch, though we do not explicitly take into account the temperature dependence of the rigidity. To some extent the choice of rigidity is arbitrary and offset by the uncertainty in the values of the tidal Qs of the early Moon and Earth.

2.2. Partial melting and melt migration in the lid

Tidal heating strongly affects the solid lid, and in these models raises parts of the lid above its melting temperature. Melting portions of the lid creates plagioclase melt migration upward in the lid, and can result in plagioclase melt eruption and re-solidification on the surface. This process has the critical effect of changing the relationship of age of the plagioclase with depth in the lid: Originally, the youngest plagioclase is at the bottom of the lid where it has floated from the remaining magma ocean, but if remelted and erupted, then the youngest plagioclase is on the surface.

Whenever some part of the lid is heated to T_p, the plagioclase there begins to melt. The melt fraction depends on the amount of heating after the temperature reaches T_p. For example, after the lid has been subjected to tidal heating and thermal diffusion for some time, a particular lid layer could reach a temperature that exceeds T_p by a positive value, ΔT, according to Eq. (4). But physically, after the layer temperature reaches T_p, the further amount of heating, ΔE, would result in melting of layer rather than further raising the layer temperature. Let V_{layer} is the volume of the layer, L_p is the latent heat in melting and crystallization of plagioclase, then $\Delta E = V_{layer}\rho_l C_p \Delta T$. The volume of the melted solid is $V_{melt} = \Delta E/(L_p\rho_l)$, so the melt fraction is

$$f_{melt} = V_{melt}/V_{layer} = (C_p/L_p)\Delta T. \tag{7}$$

We start the computation of melting in the bottom layer. Once some melt is produced, it begins to rise through the lid to the surface, thermally interacting with the lid layers that it travels through. When the melt meets a layer that is also heated to T_p

and melted to some fraction, the two bodies of melt join and migrate upward together. When the melt meets a cold layer, or a layer with a negative ΔT, some fraction crystallizes there, releasing the latent heat and increasing the layer's temperature. Meyer et al. (2010) found that the change in this fraction value from 0 to 1 does not affect the results qualitatively. We take the fraction to be 1 in this study. One exception is when the cold layer is very near T_p. In this situation, the full amount of crystallization will raise the layer temperature above T_p. Therefore, in this case we take the volume of melt crystallization to be the amount that is just enough to raise the layer temperature to T_p.

When the body of melt reaches the surface, it is instantly quenched and assumes the equilibrium surface temperature. Then any hollow in each layer caused by melting and migration is filled with material from the neighboring overlying layer or layers, with the heat content of the filling material mixed with that of the layer to be filled, thus updating the temperatures of each layer.

We take the latent heat in the melting and crystallization of plagioclase to be 4.187×10^5 J kg^{-1}, and the equilibrium surface temperature to be 280°K.

2.3. Magma ocean model

The magma ocean is assumed to be convecting and follows an adiabatic temperature profile; for the Moon this adiabatic temperature varies little with pressure and we approximate the temperature as constant with depth. Therefore, instead of tracking the full temperature profile of the magma ocean, we only track this constant temperature, T_f, and the thicknesses of the lid (δ_l), the magma ocean (δ_f), and the radius of the solid interior (δ_s), which are related to T_f in the process of magma ocean solidification.

The thermal evolution of the magma ocean is described by

$$\dot{E}_r - \dot{E}_c - L\rho_f \dot{V}_f = C_p \rho_f V_f \dot{T}_f, \tag{8}$$

where $\dot{E}_r$ is the rate of radiogenic heating of the magma ocean, $\dot{E}_c$ is the rate at which heat is conducted from the magma ocean to the lid at the base of the lid, the third term on the left hand side is the rate of production of latent heat of solidification as the volume of the magma ocean (V_f) decreases, and the right hand side is the rate of change of the heat content of the magma ocean due to its changing temperature. We take $\rho_f = 3000$ kg m^{-3}. Meyer et al. (2010) included an additional $\dot{V}_f$ related term on the right hand side to represent the change of the magma ocean's heat content due to volume decrease during solidification. However, this is compensated by the increase in heat content of the crystals settling out as their volume increases. Here we correct this error.

We compute the radiogenic heating by extrapolating the chondritic abundances of ^{235}U, ^{238}U, ^{40}K, and ^{232}Th back to the time of formation of the Moon. We then multiply by the heat production per mass, the density, and the volume of the magma ocean and sum over the four isotopes. The half-lives, current abundances, and specific heat productions are given by Turcotte and Schubert (2002).

The solidus of the magma ocean is parameterized to fit the bulk lunar mantle solidus of Longhi (2003). We use

$$T_s(r) = 2134 - 0.1724r - 1.3714 \times 10^{-4} r^2, \tag{9}$$

where T_s is the solidus in Kelvin and r is the radius in km. $T_f = T_s(\delta_s)$, so $\dot{T}_f$ can be related to $\dot{\delta}_s$:

$$\dot{T}_f = DT_s(\delta_s) \cdot \dot{\delta}_s. \tag{10}$$

Note that the solidus temperature of the magma ocean at the base of the lid, $T_s(\delta_s)$, is lower than T_p. This is because the pure mineral has a higher melting temperature than the multiphase melt has.

As the magma ocean solidifies, both plagioclase and mafic minerals crystallize from the magma. We assume constant fractional crystallization such that the volume of the crystallized plagioclase is of a fixed proportion, f, of the volume of all crystallized solids. Upon crystallization, the plagioclase floats to join the lid, while the mafic crystals precipitate on the solid interior. Let R denote the radius of the Moon, $V_l(\delta_l) = 4\pi/3(R^3 - (R-\delta_l)^3)$ denote the volume of the lid, $V_s(\delta_s) = 4\pi/3\ \delta_s{}^3$ denote the volume of the solid interior, $\dot{V}_l$ and $\dot{V}_s$ denote the rates of change of the volumes, we have

$$\dot{V}_f = -\left(\dot{V}_l + \dot{V}_s\right), \tag{11}$$

$$\dot{V}_l = f\left(\dot{V}_l + \dot{V}_s\right), \tag{12}$$

$$\dot{V}_l = 4\pi (R - \delta_l)^2 \dot{\delta}_l, \tag{13}$$

$$\dot{V}_s = 4\pi \delta_s{}^2 \dot{\delta}_s, \tag{14}$$

Putting these equations together, we find

$$\dot{\delta}_l = -\left(\dot{E}_r - \dot{E}_c\right) S_1 f/D, \tag{15}$$

$$\dot{\delta}_s = -\left(\dot{E}_r - \dot{E}_c\right) S_2 (1-f)/D, \tag{16}$$

$$\dot{T}_f = -DT_s(\delta_s)\left(\dot{E}_r - \dot{E}_c\right) S_2 (1-f)/D, \tag{17}$$

where $S_1 = 4\pi\delta_s{}^2$, $S_2 = 4\pi(R - \delta_l)^2$, $D = -C_p\rho_f S_2 V_f(\delta_l, \delta_s) DT_s(\delta_s)(1-f) + L\rho_f S_1 S_2$, the volume of the magma ocean is $V_f(\delta_l, \delta_s) = 4\pi/3((R-\delta_l)^3 - \delta_s{}^3)$. And δ_f can always be specified by $\delta_f = R - \delta_l - \delta_s$.

We tabulate the parameter values in Table 1.

3. Results

We made simulations over a range of parameters. The variation of tidal parameters can be characterized by the A parameter

$$A = \frac{k_{2M}}{Q_M} \frac{Q_E}{k_{2E}} \frac{m_E{}^2}{m_M{}^2} \frac{R_M{}^5}{R_E{}^5}, \tag{18}$$

which is a measure of the relative dissipation in the Earth and in the Moon. m_M is the mass of the Moon, R_E is the radius of the Earth.

Fig. 1 shows the angular momentum of the Earth-Moon system when the Earth-Moon distance reaches 8.5 R_E, at which point the system would have exited the limit cycle or the evection resonance if previously captured by either, versus the initial A parameter of the system. It also shows the maximum eccentricity reached in each run. For comparison, we also show the results for a non-thermally-coupled orbital model on the same figure. When the system is set such that the A parameter computed from the initial thermal state is small, in the range for evection resonance in the non-thermally-coupled model, the system does not lose angular momentum to a noticeable amount. The maximum eccentricity is 1.5–2 times smaller than that of the non-thermally-coupled counterpart, which indicates that the system does not stay long enough in the evection resonance for the eccentricity to be fully raised. On the other hand, when the initial A parameter falls in the range for the occurrence of the limit cycle, almost the same angular momentum is lost in the thermally coupled model as in the non-thermally-coupled model, and the maximum eccentricity is also similar.

First consider a case where the system is captured into the evection resonance. Fig. 2 shows the details of evolution for a run with the initial $A = 1.74$. The system gets captured in the evection

Table 1
Parameter values.

Orbital constants		Initial orbital conditions	
m_E/m_{Sun}	3.0034398×10^{-6}	*Semi-major axis*	5 R_E[c]
m_M/m_{Sun}	3.6949711×10^{-8}	*Day length*	2.53 hr[c]
R_E	1737 6371 km	*Earth's obliquity*	0
R_M	6371 1737 km	*Moon's obliquity*	0
$C_p/(m_E \cdot R_E^2)$	0.3308	*Lunar inclination*	0
ω_p	2π rad·day^{-1}	*Lunar eccentricity*	0.001
J_{2p}	0.00108263		
Thermal constants		Initial thermal conditions	
T_p	1550 °C(1823.15°K)	δ_l	5 km
C_p	1256 J kg^{-1}°K^{-1}	δ_f	110 km
L_p	4.187×10^5 J kg^{-1}	Tidal parameters	
κ	1.0×10^{-6} m^2 s^{-1}	k_{2E}	0.299
ρ_l	2927 kg m^{-3}	Q_E	400
ρ_f	3000 kg m^{-3}	k_{2M}	Determined by MO structure.
f[a]	0.4		
μ_{lid}[b]	6.5×10^9 Pa	Q_M	Determined by lunar temperature profile, and Q_{Mmin}, Q_{Mmax}.
Moon gravity	1.62 m s^{-2}		
Moon surface temperature	280°K	Q_{Mmin}	20
		Q_{Mmax}	calculated according to initial A parameter of each run.

[a] f is the plagioclase crystal proportion in magma ocean solidification.
[b] μ_{lid} is the rigidity of the lid.
[c] The combination of 5 R_E and 2.53 hr is equivalent to the combination of 3.5 R_E and 2.5 hr. We use 5 R_E and 2.53 hr in order to save some computation time.

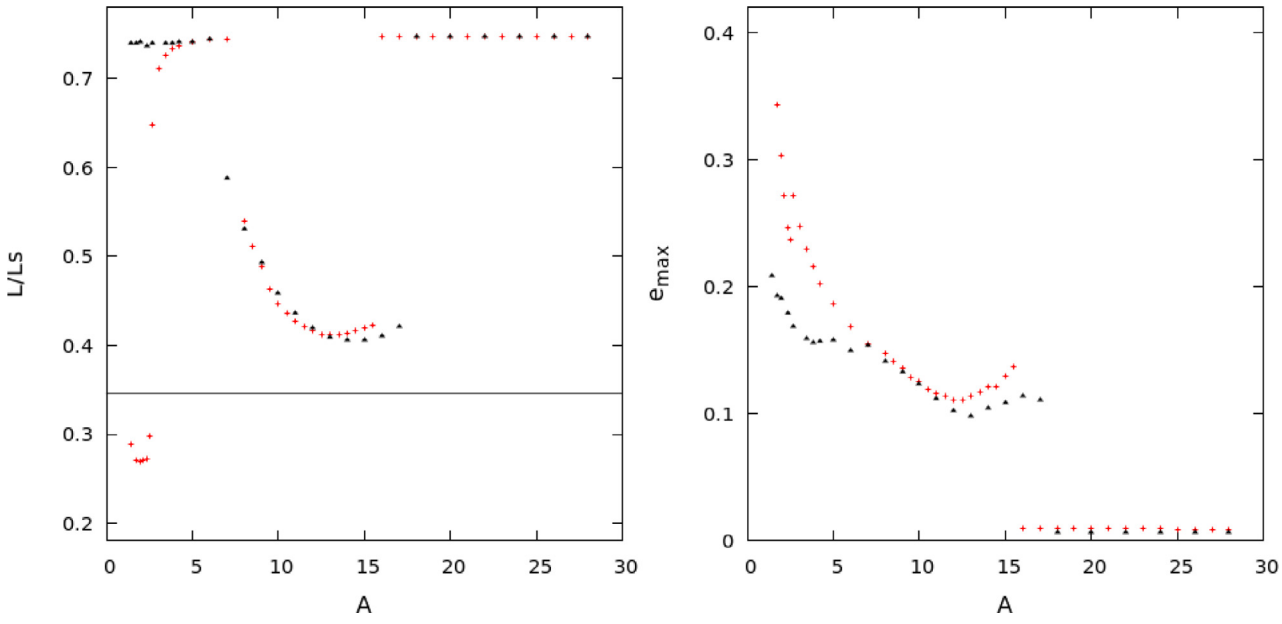

Fig. 1. Angular momentum of the Earth-Moon system when the Earth-Moon distance reaches 8.5 R_E (left) and the maximum eccentricity in each run (right) versus: (black points) the initial A parameter, for thermal-orbital coupled simulations; (red crosses) the A parameter, for non-thermally-coupled simulations. The unit of angular momentum is $L_s = C(Gm_E R_E^{-3})^{1/2}$, where G is the gravitational constant, and C is Earth's largest moment of inertia (current value). The black line is the current value of the system's angular momentum. (For interpretation of the references to colour in this figure legend, the reader is referred to the web version of this article.)

resonance at $t = 38$ thousand years (ky). Then the evection angle starts to oscillate around $\pi/2$ rad, and the lunar orbital eccentricity rises rapidly. As tidal heating gets elevated, lid temperatures gradually increase, Q of the Moon decreases, and the A parameter grows gradually. After a time lag of ~12 ky, during which the excess heat builds up in the Moon, the increase of lid temperatures is accelerated, and the A parameter grows rapidly from less than 5 to ~110. The increase of A is mainly due to the decrease in Q_M, though k_{2M} also changes. Some layers' temperatures reach T_p, so partial melting and melt migration occur. At the same time of this rapid growth of the lid temperatures and the A parameter, the system escapes the evection resonance, and the eccentricity plunges to zero. The system's exit from the resonance is due to the A parameter growing out of the range suitable for the occurrence of the resonance as observed in the non-thermally-coupled model (Fig. 1). Then as A decreases to within the range of evection resonance (~5), the system enters the evection resonance a second time. The eccentricity growth is less rapid this time, and the duration is short (~20 ky), which are consistent with the non-thermally coupled model when A is near 5 (Fig. 1, right panel, red crosses). Compared to the corresponding run with the non-thermally-coupled model, in which the system stays in the evection resonance for ~600 ky and maintains an eccentricity of ~0.34 throughout the resonance, the system in this run attains a maximum eccentricity of just 0.2, and stays in the evection resonance for only 30 ky. Therefore, the amount of angular momentum loss is negligible.

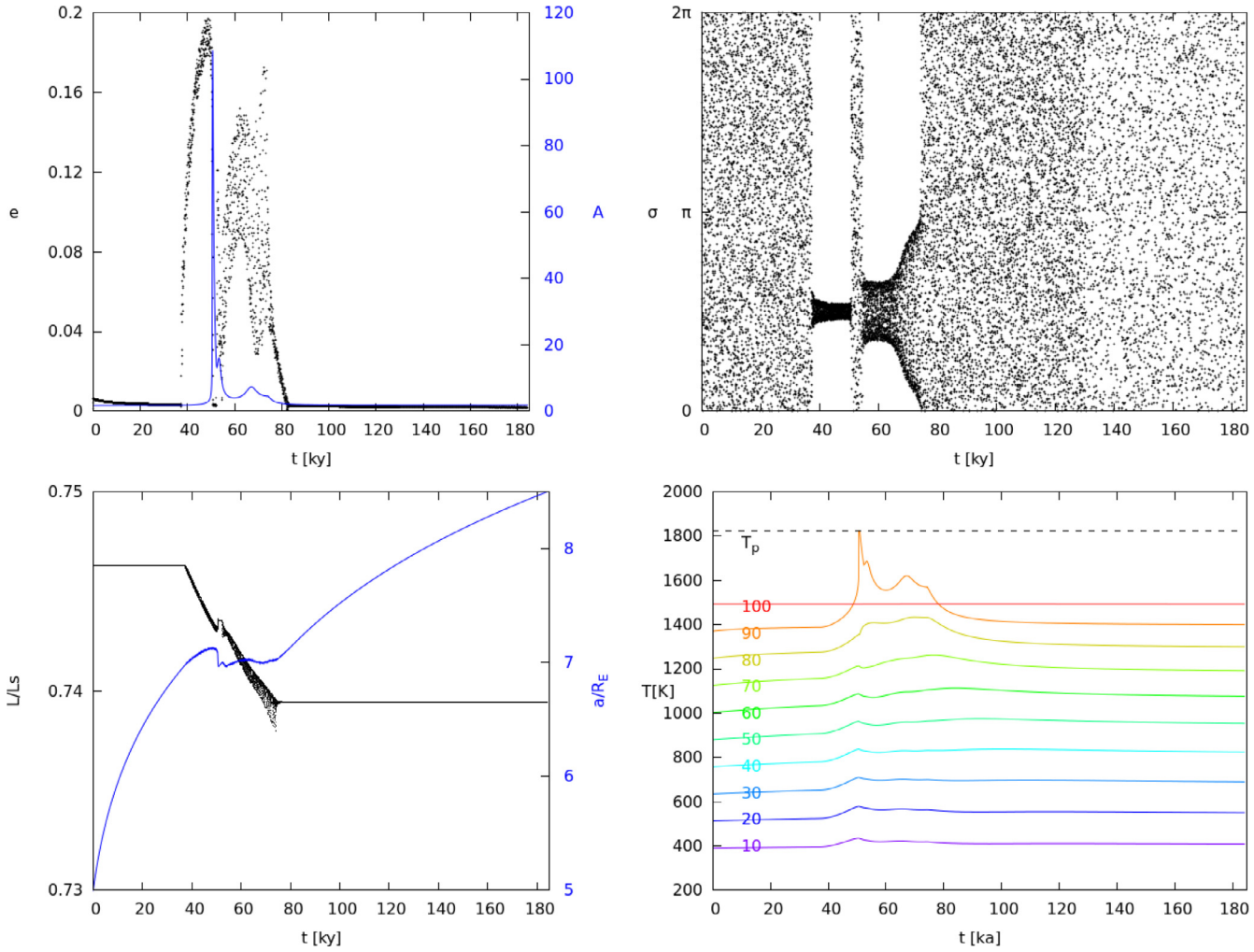

Fig. 2. The evolution of the system's A parameter (blue in upper left plot), the lunar orbit's eccentricity (black in upper left plot), the evection angle (upper right plot), the semi-major axis (in Earth radii, blue in lower left plot), the system's angular momentum (black in lower left plot), and the temperatures of selected (the 10th, 20th, … 100th) lid layers (lower right plot) for a thermal-orbital coupled simulation with an initial A parameter being 1.74. (For interpretation of the references to colour in this figure legend, the reader is referred to the web version of this article.)

The orbital and thermal processes in this run, such as the quick termination of the evection resonance and brief periods of partial melting and melt migration in the lid, are typical among the cases in which the system encounters the evection resonance.

Now consider a case where the system is captured into the limit cycle. Fig. 3 shows the details of evolution for a run with the initial $A = 14$. The system not only enters the limit cycle, but remains in the limit cycle for a long time and a significant amount of angular momentum is drained. Upon entry into the limit cycle at $t = 37$ ky, the lunar orbital eccentricity rapidly grows, as in the evection resonance. But the eccentricity oscillates between ~0.01 and ~0.09, a range whose upper bound is considerably smaller than what would be achieved in the evection resonance (0.3–0.5 in the non-thermally coupled model). Since the rate of tidal heating is approximately proportional to e^2, heating in the Moon is significantly less severe, and the growth of the A parameter is limited. As the A parameter increases, the system is still retained in the limit cycle, and the upper bound of eccentricity is lowered, which is in agreement with the trend observed in the non-thermally-coupled simulations. Then the A parameter reaches a peak value and this is when the upper bound of eccentricity stops decreasing. After that, the A parameter begins to decrease, and both bounds of the eccentricity shift upward with the change of A parameter. In the later half of the limit cycle, though the eccentricity gets as large as when the limit cycle begins, the A parameter does not increase. This is because the lid is getting increasingly more efficient at emitting heat, both to space and to the magma ocean, after the short initial phase of A increase. The detailed behavior of A is explained below.

In detail, in the beginning of the limit cycle, the large eccentricities cause elevated tidal heating in the lid, decreasing Q of the Moon and thus increasing the A parameter. But soon a maximum A value is reached, as the result of the combination of four negative feedbacks: (a) as A increases, both bounds of the eccentricity's oscillation decrease, leading to less rapid deposit of tidal heat in the lid; (b) as the temperatures of lid layers near the surface increase while the surface temperature stays constant at the equilibrium temperature, the negative temperature gradient at the surface and thus the heat flux to space increase; (c) as the temperatures of the bottom layers rise above the magma ocean temperature, heat flux switches direction (Fig. 4) so that now the lid loses some heat to the magma ocean; (d) as the heat flux at the lid base switches direction, according to Eq. (15), the lid begins to thin, while the temperatures of each layer continues to increase, so the effects of (b) and (c) get strengthened.

After A reaches the maximum, the lid continues to thin as the bottom layers continue to be hotter than the magma ocean. So even though the lid temperatures have stopped increasing, (d) con-

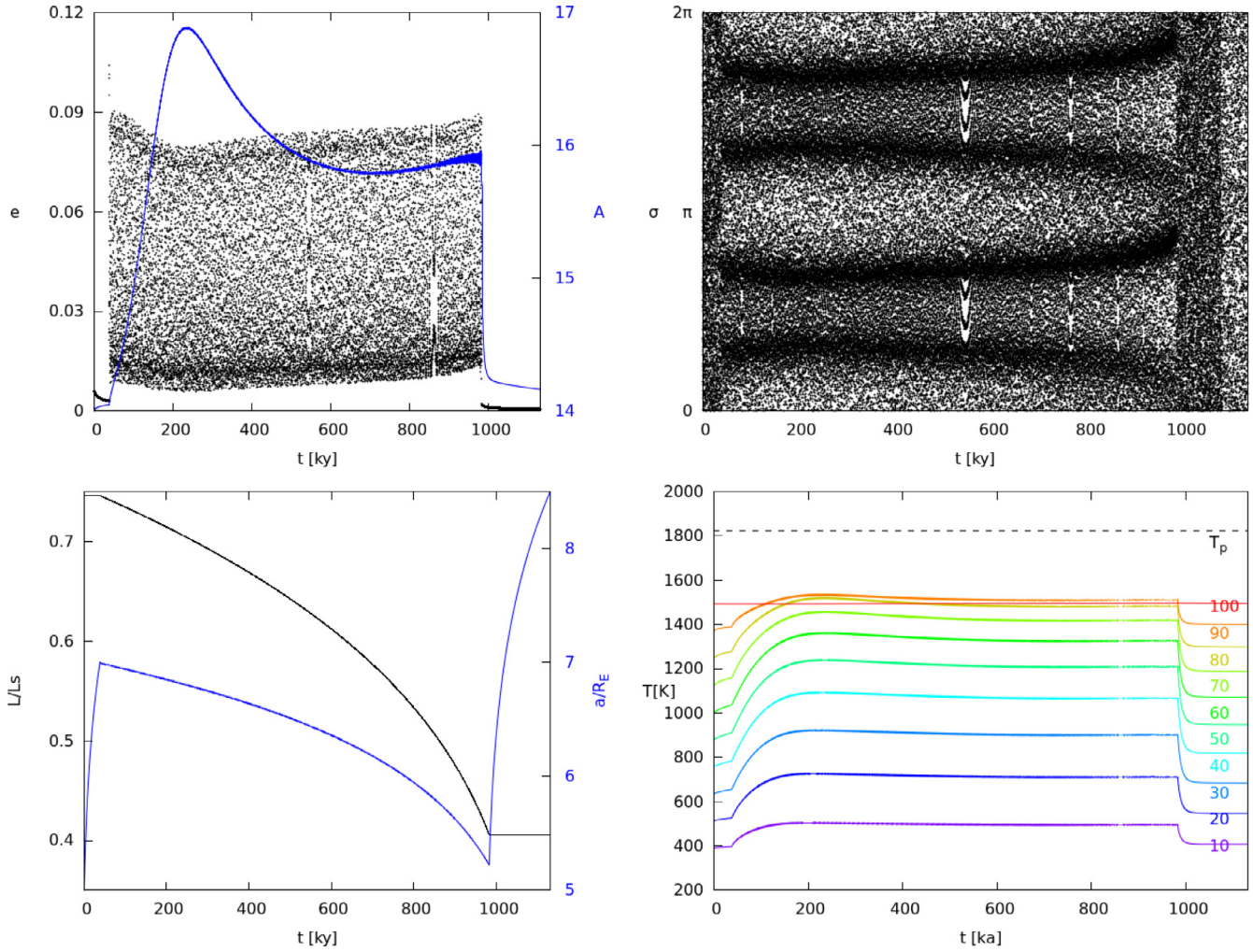

Fig. 3. The evolution of the same parameters as in Fig. 2, for a thermal-orbital coupled simulation with an initial *A* parameter being 14.

tinues at work, strengthening (b). Then the rate of heat loss from the lid, now dominated by (d) and (b), exceeds the rate of heat deposit in the lid, and the lid temperatures begin to decrease, causing the *A* parameter to decrease, too. But as *A* decreases, the range of eccentricity oscillation gets to higher values, thus slowing down the rate of decrease of *A*.

In the later half the limit cycle, two opposing mechanisms work simultaneously: (i) the thinning of the lid leads to an increasing rate of heat loss from the lid mainly through (d) and (b), and (ii) the resultant decrease of *A* leads to an increasing rate of tidal heating in the lid (through increase eccentricities) which slows down the decrease of *A*, acting as a negative feedback on (i). The result is that A approaches an asymptotic value, as shown in Fig. 3.

The system remains in the limit cycle in the whole process even though the *A* parameter changes, allowing the continued draining of angular momentum from the Earth-Moon system. This robustness is partly attributed to the range of *A* parameter that allows the occurrence and maintenance of the limit cycle being much wider than that for the evection resonance.

4. Discussion and conclusion

We also carried out simulations with Q_E being 200, 300 and 500, and other parameters kept the same. Results are shown in Fig. 5 as angular momentum versus the initial *A* parameter. We see that at all Q_E values there is no significant angular momentum decrease in the evection resonance region (*A* in 1–3), consistent with what we observed for the $Q_E = 400$ case. The results also show that when a smaller Q_E (300) is used, the limit cycle is still encountered, but over a smaller range of parameters. When Q_E is further decreased to 200, no observable angular momentum decrease occurs, indicating the absence of the system's capture in the limit cycle. This trend illustrates the importance of Q_E in the Earth-Moon system's early evolution: Q_E controls the rate of Earth-Moon separation, and the limit cycle, as well as resonances, capture the system with a higher chance when the Moon is separating from the Earth at a lower rate. A small Q_E means larger tidal disturbing forces to the system, which makes it harder for the limit cycle to occur and to be maintained. Zahnle et al. (2007) preferred a large Q_E, which can better facilitate angular momentum loss in our model.

These results also demonstrate the importance of the *A* parameter in the early evolution of the Earth-Moon system. As long as the Earth-Moon separation is sufficiently slow (by assuming a sufficiently large Q_E), the system enters the limit cycle at the same *A* parameter values. Thus the detailed values of *Q* and k_2 are less important.

With the orbital evolution of the Earth-Moon system being coupled with the thermal evolution of the Moon, and beginning with a fast spinning Earth, the system cannot lose its excess angular

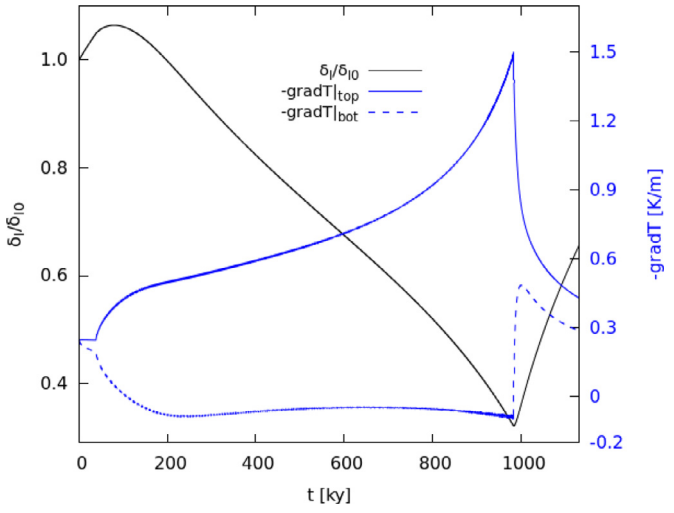

Fig. 4. The evolution of the lid thickness (black curve, left scale) and temperature gradients at the top (blue solid curve, right scale) and the bottom (blue dashed curve, right scale) of the lid, for the same simulation as in Fig. 3. The lid thickness is normalized with the initial thickness. (For interpretation of the references to colour in this figure legend, the reader is referred to the web version of this article.)

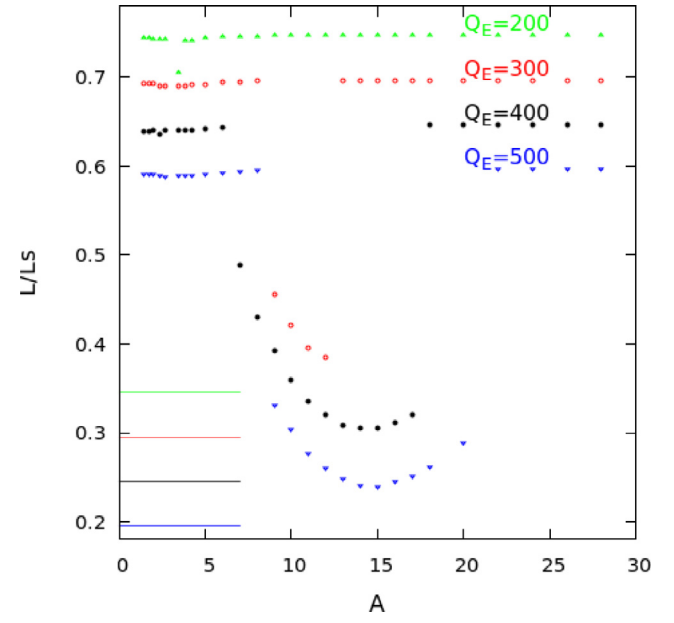

Fig. 5. The system's angular momentum when the Earth-Moon distance reaches 8.5 R_E, versus the initial A parameter, for the cases of Q_E=200 (green), Q_E=300 (red), Q_E=400 (black), Q_E=500 (blue). The Q_E=300, Q_E=400 and Q_E=500 points are offset by –0.05, –0.10 and –0.15 on the y-axis respectively to improve clarity. The lines of current angular momentum are also offset accordingly. (For interpretation of the references to colour in this figure legend, the reader is referred to the web version of this article.)

momentum through the evection resonance. When the system encounters the evection resonance, the eccentricity tends to be excited to large values (0.3–0.5), tidal heating in the lid becomes too intense to be efficiently conducted out, and partial melting and melt migration occur. The severe heating during the resonance induces rapid changes in the Moon's tidal properties and thus in the tidal accelerations, forcing the system to exit the resonance soon after it enters the resonance. In contrast, due to the lower eccentricities and the effects of feedback mechanisms that reduce the net heating in the lid, the limit cycle mechanism works stably over extended periods of time, and successfully reduces the Earth-Moon system's angular momentum to a value that is near the current value over a wide range of parameters. Therefore, we conclude that if the Moon formed in a giant impact scenario that leaves the early Earth spinning much faster than is deduced from the current Earth-Moon's angular momentum, the limit cycle is a viable mechanism to have removed the excess angular momentum.

Appendix: tidal heating in a synchronously rotating, two-layered satellite

The issue of tidal heating in a shell has been studies by previous investigators (Peale and Cassen, 1978; Peale et al., 1979; Wahr et al., 2006; Meyer et al., 2010; Beuthe, 2013). For convenience, we derive the expression of degree-2 tidal heating in synchronously rotating, two-layered satellite. The solid exterior layer of the satellite has a much higher shear rigidity than the liquid interior layer ($\mu^E \gg \mu^l$). Both layers are incompressible and have the same density. We use the constant-Q Darwin–Kaula formulation to model the tide. In part 1, we derive the equations of the equilibrium displacement in the satellite and the boundary conditions. In part 2, we solve the displacement field and derive the equilibrium strain. In part 3, we derive tidal heating as a function of position in the satellite, the angle-averaged heating at a given radius, and the total heating in the outer solid layer of the satellite.

1: equation of displacement, boundary conditions

To establish the equation of the equilibrium displacement, we need to analyze the forces in the satellite in the presence of a gravitational perturber. The forces are:

(i) hydrostatic pressure ($-p_0$, p_0 is positive when the pressure is compressive);
(ii) satellite's self gravitational acceleration when unperturbed ($-g_r\,\hat{r}$);
(iii) stress caused by tidal distortion ($\bar{\bar{X}}$);
(iv) forces from the total disturbing potential (∇U, U is defined after Eq. (a1)).

(i), (ii) satisfy (as when the satellite is unperturbed):

$$-\nabla p_0 - \rho g_r \hat{r} = 0$$

(i), (ii), (iii), (iv) satisfy the equilibrium equation (Love 1944, pp.257, eq. 23):

$$-\nabla p_0 + \nabla \cdot \bar{\bar{X}} - \rho g_r \hat{r} + \rho \nabla U = 0$$

the two equations give

$$\nabla \cdot \bar{\bar{X}} + \rho \nabla U = 0.$$

In Cartesian coordinates, the x component is:

$$\partial_x X_{xx} + \partial_y X_{xy} + \partial_z X_{xz} + \rho \times \partial_x U = 0 \qquad (a1)$$

U, the total disturbing potential, is the sum of the perturber's disturbing potential and the potential associated with the satellite's distortion. It can be spherical harmonically expanded. According to Love 1944 (pp.257, eq. 22),

$$U = \Sigma_n U_n$$
$$= \Sigma_n \left[V_n + 3g/(2n+1) \times \Delta_n \times (r/R)^n \right],$$

where Δ_n is the degree-n radial displacement at the satellite's surface, g is the surface gravitational acceleration, r is the radius of the point of evaluation, and R is the satellite's radius.

$$V_n = GM\left(r/r'\right)^n P_n(\cos S),$$

where G is the gravitational constant, M is the mass of the planet, S is the angle between the direction of the perturber from the center of the satellite and the direction to the point of evaluation, r' is the distance between the satellite and the planet. Define

$V_n^0 = GMr'^{-n-1}R^n$, then

$V_n = V_n^0 \cdot (r/R)^n P_n(\cos S)$, and the corresponding surface radial displacement takes the form

$\Delta_n = \Delta_n^0 P_n(\cos S)$. So

$$U_n = \left[V_n^0 + 3g/(2n+1)\cdot\Delta_n^0\right] \times (r/R)^n P_n(\cos S). \quad (a2)$$

With the definition of the degree n potential Love number k_n as

$U_n = V_n + k_n \times V_n$ (where $r \le R$),

we have

$$k_n = 3g/(2n+1)\Delta_n^0/V_n^0. \quad (a3)$$

Now we relate (1) to the displacement field. Since

$$X_{ij} = -p\delta_{ij} + 2\mu e_{ij}, \quad (a4)$$

where p is the mean pressure due to tidal distortion, and in rectangular coordinates,

$$e_{ij} = 1/2\left(\partial_i u_j + \partial_j u_i\right),$$

we can rewrite (1) as

$$-\partial_x(p-\rho U) + \mu(\partial_x\partial_x + \partial_y\partial_y + \partial_z\partial_z)u_x + \mu\partial_x(\partial_x u_x + \partial_y u_y + \partial_z u_z) = 0. \quad (a5)$$

The incompressible assumption gives

$$\nabla\cdot\vec{u} = 0 \quad (a6)$$

$$\text{Define } P = p - \rho U, \quad (a7)$$

then (5) and (6) give

$$-\nabla P + \mu\nabla^2\vec{u} = 0. \quad (a8)$$

Since μ is constant in each layer, (a2), (a6) and (a8) imply that P is a harmonic function (i.e., $\nabla^2 P = 0$). Then (a8) can be expanded as:

$$-\nabla P_{n\pm} + \mu\nabla^2\vec{u}_{n\pm} = 0, \quad (a9)$$

where

$$P_{n+} = P_{n+}^0 (r/R)^n P_n(\cos S) = p_{n+} - \rho U_n,$$

$$P_{n-} = P_{n-}^0 (r/R)^{-n-1} P_n(\cos S) = p_{n-}$$

in the outer layer, and

$$P_{n+} = P_{ln}^0 (r/R)^n P_n(\cos S),$$

$$P_{n-} = 0$$

in the inner layer.

A particular solution is given by Love 1944 (p. 258):

$$\overrightarrow{u_{Pn\pm}} = A_{n\pm} r^2 \nabla P_{n\pm} + B_{n\pm}\vec{r}\, P_{n\pm}$$

where $A_{n\pm}$, $B_{n\pm}$ satisfy

$$(4k_\pm + 2)A_{n\pm} + 2B_{n\pm} = \mu^{-1},$$
$$2k_\pm A_{n\pm} + (k_\pm + 3)B_{n\pm} = 0,$$
$$k_+ = n,\ k_- = -(n+1),$$
$$(A_{2+} = 5/42\,\mu^{-1}, B_{2+} = -2/21\mu^{-1}, A_{2-} = 0, B_{2-} = 1/2\mu^{-1}),$$

where μ is the rigidity of whichever zone is under consideration. We use μ^E to denote the rigidity of the outer layer and μ^I for the inner layer.

Following Peale and Cassen 1978, we take the homogeneous solution to be

$$\overrightarrow{u_{Hn\pm}} = \nabla\times(\vec{r}\times\nabla\Phi_{n\pm})$$

where $\Phi_{n\pm}$ is any harmonic function. The harmonic coefficients Φ^0_{n+}, Φ^0_{n-} and Φ^0_{ln} are defined similarly to those for $P_{n\pm}$.

The complete solution is

$$\overrightarrow{u_n} = \overrightarrow{u_{n+}} + \overrightarrow{u_{n-}}$$
$$\overrightarrow{u_{n\pm}} = A_{n\pm} r^2\nabla^2 P_{n\pm} + B_{n\pm}\vec{r}P_{n\pm} - \nabla(\Phi_{n\pm} + \vec{r}\cdot\nabla\Phi_{n\pm}) \quad (a10)$$

Now we specify the boundary conditions.

At the satellite's deformed surface, total traction vanishes:

$$(X_{rr} - p_0)|_{r=R} + \Delta\cdot[\partial_r(X_{rr} - p_0)]|_{r=R} = 0,$$
$$X_{r\theta}|_{r=R} + \Delta\cdot\partial_r X_{r\theta}|_{r=R} = 0,$$
$$X_{r\phi}\big|_{r=R} + \Delta\cdot\partial_r X_{r\phi}\big|_{r=R} = 0,$$

where Δ is the sum of Δ_n. Note that $p_0|_{r=R} = 0$, $\partial_r p_0 = -\rho g$. $X_{ri} = -p\delta_{ri} + 2\mu e_{ri}$, $p = O(\mu\cdot\Delta/R)$, $e_{ri} = O(\Delta/R)$, so $X_{ri} = O(\Delta/R)$, $\Delta\cdot\partial_r X_{ri}|_{r=R} = O(\Delta/R)^2$. Neglect terms of $O(\Delta R/R)^2$ and higher, we get

$$X_{rr}|_{r=R} + \rho g\Delta = 0, \quad (a11)$$

$$X_{r\theta}|_{r=R} = 0. \quad (a12)$$

The $X_{r\phi}$ equation is neglected because it gives the same constraint as the $X_{r\theta}$ equation.

The total traction is continuous at the boundary between the two layers:

$$(X_{rr} - p_0)|_{r=R} + \Delta\cdot[\partial_r(X_{rr} - p_0)]|_{r=b-} = (X_{rr} - p_0)|_{r=R} + \Delta\cdot[\partial_r(X_{rr} - p_0)]|_{r=b+},$$
$$X_{r\theta}|_{r=b-} + \Delta\cdot\partial_r X_{r\theta}|_{r=b-} = X_{r\theta}|_{r=b+} + \Delta\cdot\partial_r X_{r\theta}|_{r=b+}.$$

We assume the two layers have the same density, so $\partial_r p_0|_{r=b-} = \partial_r p_0|_{r=b+} = -\rho g$. Neglect of $O(\Delta R/R)^2$ and higher terms gives:

$$X_{rr}|_{r=b-} = X_{rr}|_{r=b+}, \quad (a13)$$

$$X_{r\theta}|_{r=b-} = X_{r\theta}|_{r=b+}. \quad (a14)$$

The displacement components are also continuous at the boundary:

$$u_r|_{r=b-} = u_r|_{r=b+}, \quad (a15)$$

$$u_\theta|_{r=b-} = u_\theta|_{r=b+}. \quad (a16)$$

We also have Δ being the radial displacement at r=R:

$$u_r|_{r=R} = \Delta. \quad (a17)$$

2: solution of displacement and strain

We can transform the conditions on the traction to conditions on the displacement using the relation:

$$\mu^{-1}\mathrm{r}\overrightarrow{\mathrm{X}_\mathrm{r}} = -\mu^{-1}(\mathrm{P}+\rho\mathrm{U})\ \vec{\mathrm{r}}+\nabla(\vec{\mathrm{r}}\cdot\vec{\mathrm{u}})+(\vec{\mathrm{r}}\cdot\nabla)\vec{\mathrm{u}}\ -\vec{\mathrm{u}}, \qquad (a18^1)$$

where $\vec{\mathrm{X}}_\mathrm{r} = \overline{\overline{\mathrm{X}}}\cdot\hat{r}$. Use of (a2), (a10) and (18) in boundary conditions (a11)~(a17) leads to a set of linear equations for $\mu^{\mathrm{E}}\Phi_{2+}{}^0$, $\mu^{\mathrm{E}}\Phi_{2-}{}^0$, $\mathrm{R}^2\mathrm{P}_{2+}{}^0$, $\mathrm{R}^2\mathrm{P}_{2-}{}^0$, $\mu^{\mathrm{I}}\Phi_{\mathrm{I}2}{}^0$, $\mathrm{R}^2\mathrm{P}_{\mathrm{I}2}{}^0$, and $\mu^{\mathrm{E}}\mathrm{R}\Delta_2{}^0$. The matrix of coefficients is

$$\begin{array}{cccccccc}
-12 & 48 & -1/7 & -3 & 0 & 0 & \frac{2}{5}\frac{\rho g R}{\mu^{\mathrm{E}}} & \rho\mathrm{R}^2\mathrm{V}_2^0 \\
-6 & -16 & 8/21 & 1/2 & 0 & 0 & 0 & 0 \\
-12\eta^2 & 48\eta^{-3} & -\eta^4/7 & -3\eta^{-1} & 12\eta^2 & \frac{1}{7}\eta^4 & 0 & 0 \\
-6\eta^2 & -16\eta^{-3} & \frac{8}{21}\eta^4 & 1/2\eta^{-1} & 6\eta^2 & \frac{-8}{21}\eta^4 & 0 & 0 \\
-6\eta^2 & -6\eta^3 & \eta^4/7 & 1/2\eta^{-1} & 6\eta^2\beta & \frac{-1}{7}\eta^4\beta & 0 & 0 \\
-3\eta^2 & 2\eta^{-3} & \frac{5}{42}\eta^4 & 0 & 3\eta^2\beta & \frac{-5}{42}\eta^4\beta & 0 & 0 \\
-6 & -6 & 1/7 & 1/2 & 0 & 0 & -1 & 0
\end{array} \qquad (a19)$$

where $\eta = \mathrm{b}/\mathrm{R}$, b is the radius of the boundary between two layers, and $\beta = \mu^{\mathrm{E}}/\mu^{\mathrm{I}}$. Since the inner layer is liquid, we take the limit $\beta -> \infty$. Then the two lines in (a19) dominated by β terms imply that $\mu^{\mathrm{I}}\Phi_{\mathrm{I}2}{}^0 = \mathrm{R}^2\mathrm{P}_{\mathrm{I}2}{}^0 = 0$. So we ignore these two variables, and hereafter use μ to refer to μ^{E} since μ^{I} does not appear. The solutions of the other variables are:

$$\begin{aligned}
\mu\Phi^0_{2+} &= \mu\mathrm{R}\Delta^0_2(5\xi)^{-1} \\
&\quad\cdot(-32\eta_{012}-32\eta_{34}-60\eta_{56}), \\
\mu\Phi^0_{2-} &= \mu\mathrm{R}^0_2(5\xi)^{-1} \\
&\quad\cdot(32\eta_{56}+19/2\eta_{789}), \\
\mathrm{R}^2\mathrm{P}^0_{2+} &= \mu\mathrm{R}\Delta^0_2(5\xi)^{-1} \\
&\quad\cdot(-504\eta_{012}-1344\eta_{34}), \\
\mathrm{R}^2\mathrm{P}^0_{2-} &= \mu\mathrm{R}\Delta^0_2(5\xi)^{-1} \\
&\quad\cdot(640\eta_{34}+304\eta_{56}+304\eta_{789}),
\end{aligned} \qquad (a20)$$

and

$$\mu\mathrm{R}\Delta^0_2 = \rho\mathrm{R}^2\mathrm{V}^0_2(5\xi)/[2\xi\cdot\rho g\mathrm{R}/\mu+24\lambda], \qquad (a21)$$

where

$$\begin{aligned}
\xi &= 24\eta_{012}+64\eta_{34}+64\eta_{56}+19\eta_{789}, \\
\lambda &= 19\eta_{012}-56\eta_{34}+56\eta_{56}-19\eta_{789}, \\
\eta_{012} &= 1+\eta+\eta^2, \\
\eta_{34} &= \eta^3+\eta^4, \\
\eta_{56} &= \eta^5+\eta^6, \\
\eta_{789} &= \eta^7+\eta^8+\eta^9.
\end{aligned}$$

From (a3) and (a21)

$$\mathrm{k}_2 = 3\mathrm{g}/5\Delta^0_2/\mathrm{V}^0_2 = \frac{\frac{3}{2}\xi}{\xi+12\lambda\ \mu/(\rho g\mathrm{R})}. \qquad (a22^2)$$

We note that $\mu\mathrm{R}\Delta_2{}^0 = 5/3$ $(\mathrm{g}^{-1}\mu\mathrm{R}\mathrm{k}_2\mathrm{V}_2{}^0)$. Since $\mu\Phi_{2+}{}^0$, $\mu\Phi_{2-}{}^0$, $\mathrm{R}^2\mathrm{P}_{2+}{}^0$, $\mathrm{R}^2\mathrm{P}_{2-}{}^0$ are all ratios of $\mu\mathrm{R}\Delta_2{}^0$, they are also ratios of $(\mathrm{g}^{-1}\mu\mathrm{R}\mathrm{k}_2\mathrm{V}_2{}^0)$, and the ratios are functions of η, as shown in (a20).

Substitution of these coefficients into (a10) gives the displacement solution:

$$\begin{aligned}
\mathrm{u}_\mathrm{r} &= \mathrm{R}\mathrm{g}^{-1}\mathrm{k}_2\alpha_1(\mathrm{r}^{-1}\mathrm{V}_2), \\
\mathrm{u}_\theta &= \mathrm{R}\mathrm{g}^{-1}\mathrm{k}_2\alpha_2(\mathrm{r}^{-1}\partial_\theta\mathrm{V}_2), \\
\mathrm{u}_\phi &= \mathrm{R}\mathrm{g}^{-1}\mathrm{k}_2\alpha_2(\mathrm{r}^{-1}\sin^{-1}\theta\cdot\partial_\phi\mathrm{V}_2),
\end{aligned} \qquad (a23)$$

where

$$\begin{aligned}
\alpha_1 = 2/3\xi^{-1}\big[&(-96\eta_{56}-57/2\eta_{789})\mathrm{r}_1^{-5} \\
&+(160\eta_{34}+76\eta_{56}+76\eta_{789})\mathrm{r}_1^{-3} \\
&+(96\eta_{012}+96\eta_{34}+180\eta_{56}) \\
&+(-36\eta_{012}-96\eta_{34})\mathrm{r}_1^2\big], \\
\alpha_2 = 2/3\xi^{-1}\big[&(32\eta_{56}+19/2\eta_{789})\mathrm{r}_1^{-5} \\
&+(48\eta_{012}+48\eta_{34}+90\eta_{56}) \\
&+(-30\eta_{012}-80\eta_{34})\mathrm{r}_1^2\big].
\end{aligned} \qquad (a24^3)$$

The equilibrium strain is the spatial derivative of the equilibrium displacement. In Cartesian coordinates, $\mathrm{e}_{\mathrm{ij}} = \frac{1}{2}(\partial_\mathrm{i}\mathrm{u}_\mathrm{j}+\partial_\mathrm{j}\mathrm{u}_\mathrm{i})$. In arbitrary curvilinear coordinates (α, β, γ), the relation between strain and displacement is

$$\begin{aligned}
\mathrm{e}_{\alpha\alpha} &= \mathrm{h}_\alpha\partial_\alpha\mathrm{u}_\alpha+\mathrm{h}_\alpha\mathrm{h}_\beta\mathrm{u}_\beta\partial_\beta(1/\mathrm{h}_\alpha)+\mathrm{h}_\gamma\mathrm{h}_\alpha\mathrm{u}_\gamma\partial_\gamma(1/\mathrm{h}_\alpha) \\
\mathrm{e}_{\beta\beta} &= \mathrm{h}_\beta\partial_\beta\mathrm{u}_\beta+\mathrm{h}_\beta\mathrm{h}_\gamma\mathrm{u}_\gamma\partial_\gamma\left(1/\mathrm{h}_\beta\right)+\mathrm{h}_\alpha\mathrm{h}_\beta\mathrm{u}_\alpha\partial_\alpha\left(1/\mathrm{h}_\beta\right) \\
\mathrm{e}_{\gamma\gamma} &= \mathrm{h}_\gamma\partial_\gamma\mathrm{u}_\gamma+\mathrm{h}_\gamma\mathrm{h}_\alpha\mathrm{u}_\alpha\partial_\alpha\left(1/\mathrm{h}_\gamma\right)+\mathrm{h}_\beta\mathrm{h}_\gamma\mathrm{u}_\beta\partial_\beta\left(1/\mathrm{h}_\gamma\right) \\
\mathrm{e}_{\alpha\beta} &= 1/2[\mathrm{h}_\alpha/\mathrm{h}_\beta\cdot\partial_\alpha\left(\mathrm{h}_\beta\mathrm{u}_\beta\right)+\mathrm{h}_\beta/\mathrm{h}_\alpha\cdot\partial_\beta(\mathrm{h}_\alpha\mathrm{u}_\alpha)] \\
\mathrm{e}_{\beta\gamma} &= 1/2[\mathrm{h}_\beta/\mathrm{h}_\gamma\cdot\partial_\beta\left(\mathrm{h}_\gamma\mathrm{u}_\gamma\right)+\mathrm{h}_\gamma/\mathrm{h}_\beta\cdot\partial_\gamma\left(\mathrm{h}_\beta\mathrm{u}_\beta\right)] \\
\mathrm{e}_{\gamma\alpha} &= 1/2[\mathrm{h}_\gamma/\mathrm{h}_\alpha\cdot\partial_\gamma(\mathrm{h}_\alpha\mathrm{u}_\alpha)+\mathrm{h}_\alpha/\mathrm{h}_\gamma\cdot\partial_\alpha\left(\mathrm{h}_\gamma\mathrm{u}_\gamma\right)]
\end{aligned} \qquad (a25)$$

where $\mathrm{h}_\alpha = |\nabla\alpha|$, $\mathrm{h}_\beta = |\nabla\beta|$, $\mathrm{h}_\gamma = |\nabla\gamma|$.

In spherical coordinates (r, θ, ϕ),

$$\mathrm{h}_\mathrm{r} = 1,\ \mathrm{h}_\theta = \mathrm{r}^{-1},\ \mathrm{h}_\phi = \mathrm{r}^{-1}\sin^{-1}\theta. \qquad (a26)$$

Substitution of (a23) and (a26) in (a25) gives

$$\begin{aligned}
\mathrm{e}_{\mathrm{rr}} &= \mathrm{R}\mathrm{g}^{-1}\mathrm{k}_2\cdot\mathrm{A}\alpha_0, \\
\mathrm{e}_{\theta\theta} &= \mathrm{R}\mathrm{g}^{-1}\mathrm{k}_2\cdot(\mathrm{A}\alpha_1+\mathrm{B}\alpha_2), \\
\mathrm{e}_{\phi\phi} &= \mathrm{R}\mathrm{g}^{-1}\mathrm{k}_2\cdot(\mathrm{A}\alpha_1+\mathrm{C}\alpha_2), \\
\mathrm{e}_{\mathrm{r}\theta} &= \mathrm{R}\mathrm{g}^{-1}\mathrm{k}_2\cdot\mathrm{D}\alpha_3, \\
\mathrm{e}_{\theta\phi} &= \mathrm{R}\mathrm{g}^{-1}\mathrm{k}_2\cdot\mathrm{E}\alpha_2, \\
\mathrm{e}_{\mathrm{r}\phi} &= \mathrm{R}\mathrm{g}^{-1}\mathrm{k}_2\cdot\mathrm{H}\alpha_3,
\end{aligned} \qquad (a27)$$

where

$$\begin{aligned}
\mathrm{A} &= \mathrm{r}^{-2}\mathrm{V}_2 = \mathrm{GMr}'^{-3}\mathrm{P}_2(\cos\mathrm{S}), \\
\mathrm{B} &= \partial_\theta\partial_\theta\mathrm{A}, \\
\mathrm{C} &= \sin^{-2}\theta\cdot\partial_\phi\partial_\phi\mathrm{A}+\cot\theta\cdot\partial_\theta\mathrm{A}, \\
\mathrm{D} &= \partial_\theta\mathrm{A}, \\
\mathrm{E} &= \sin^{-1}\theta\cdot\partial_\phi(\partial_\theta\mathrm{A}-\cot\theta\cdot\mathrm{A}), \\
\mathrm{H} &= \sin^{-1}\theta\cdot\partial_\phi\mathrm{A},
\end{aligned} \qquad (a28)$$

[1] Proof: From (a25), (a26), (a4) and (a7), we have
$\mathrm{X}_{\mathrm{rr}} = -(\mathrm{P}+\rho\mathrm{U})+2\mu\partial_\mathrm{r}\mathrm{u}_\mathrm{r}$,
$\mathrm{X}_{\mathrm{r}\theta} = \mu(\mathrm{r}\cdot\partial_\mathrm{r}(\mathrm{r}^{-1}\mathrm{u}_\theta)+\mathrm{r}^{-1}\partial_\theta\mathrm{u}_\mathrm{r})$,
$\mathrm{X}_{\mathrm{r}\phi} = \mu(\mathrm{r}^{-1}\sin^{-1}\theta\cdot\partial_\phi\mathrm{u}_\mathrm{r}+\mathrm{r}\cdot\partial_\mathrm{r}(\mathrm{r}^{-1}\mathrm{u}_\phi))$.
Since $\vec{\mathrm{X}}_\mathrm{r} = \mathrm{X}_{\mathrm{rr}}\hat{\mathrm{r}}+\mathrm{X}_{\mathrm{r}\theta}\hat{\theta}+\mathrm{X}_{\mathrm{r}\phi}\hat{\phi}$, we get
$\vec{\mathrm{X}}_\mathrm{r}+(\mathrm{P}+\rho\mathrm{U})\hat{\mathrm{r}} = 2\mu\partial_\mathrm{r}\mathrm{u}_\mathrm{r}\hat{\mathrm{r}}+\mu[\mathrm{r}\partial_\mathrm{r}(\mathrm{r}^{-1}\mathrm{u}_\theta)+\mathrm{r}^{-1}\partial_\theta\mathrm{u}_\mathrm{r}]\hat{\theta}$
$+\mu[\mathrm{r}^{-1}\sin^{-1}\theta\cdot\partial_\phi\mathrm{u}_\mathrm{r}+\mathrm{r}\partial_\mathrm{r}(\mathrm{r}^{-1}\mathrm{u}_\phi)]\hat{\phi}$.
Apply the relation: $\mathrm{r}\partial_\mathrm{r}(\mathrm{r}^{-1}\mathrm{u}_\mathrm{r}) = -\mathrm{r}^{-1}\mathrm{u}_\mathrm{r}+\partial_\mathrm{r}\mathrm{u}_\mathrm{r}$, and multiply both sides with $\mu^{-1}\mathrm{r}$, we get:
$\mu^{-1}\mathrm{r}\vec{\mathrm{X}}_\mathrm{r}+\mu^{-1}(\mathrm{P}+\rho\mathrm{U})\vec{\mathrm{r}}$
$= \mathrm{r}[\partial_\mathrm{r}\mathrm{u}_\mathrm{r}\hat{\mathrm{r}}+\mathrm{r}^{-1}\partial_\theta\mathrm{u}_\mathrm{r}\hat{\theta}+\mathrm{r}^{-1}\sin^{-1}\theta\cdot\partial_\phi\mathrm{u}_\mathrm{r}\hat{\phi}]$
$+\mathrm{r}\cdot\mathrm{u}_\mathrm{r}\hat{\mathrm{r}}+\mathrm{r}^2[\partial_\mathrm{r}(\mathrm{r}^{-1}\mathrm{u}_\mathrm{r})\hat{\mathrm{r}}+\partial_\mathrm{r}(\mathrm{r}^{-1}\mathrm{u}_\theta)\hat{\theta}+\partial_\mathrm{r}(\mathrm{r}^{-1}\mathrm{u}_\phi)\hat{\phi}]$
$= \mathrm{r}(\nabla\mathrm{u}_\mathrm{r}+\mathrm{u}_\mathrm{r}\nabla\mathrm{r})+\mathrm{r}^2\partial_\mathrm{r}(\mathrm{r}^{-1}\vec{\mathrm{u}})$
$= \nabla(\mathrm{r}\cdot\mathrm{u}_\mathrm{r})-\vec{\mathrm{u}}+\mathrm{r}\partial_\mathrm{r}\vec{\mathrm{u}}$
$= \nabla(\vec{\mathrm{r}}\cdot\vec{\mathrm{u}})-\vec{\mathrm{u}}+(\vec{\mathrm{r}}\cdot\nabla)\vec{\mathrm{u}}$.(a18) is proven.

[2] When η=0, we get ξ=24, λ=19, $\mathrm{k}_2 = \frac{3/2}{1+(19/2)\ \mu/(\rho g\mathrm{R})}$.

[3] When η=0, α_1=8/3 -$\mathrm{r}_1{}^2$, α_2 =4/3 -5/6 $\mathrm{r}_1{}^2$. Note that $\mathrm{k}_2\cdot\alpha_1$ is equivalent to $\mathrm{k}_2'\cdot\alpha_2$ in Peale & Casen (1978) and Meyer (2010), and that $\mathrm{k}_2\cdot\alpha_2$ is equivalent to their $\mathrm{k}_2'\cdot\alpha_1$.

which are all independent of r, and

$$\begin{aligned}\alpha_0 &= \partial_r(r\cdot\alpha_1)\\ &= 2/3\xi^{-1}\big[(384\eta_{56}+114\eta_{789})r_1^{-5}\\ &\quad+(-320\eta_{34}-152\eta_{56}-152\eta_{789})r_1^{-3}\\ &\quad+(96\eta_{012}+96\eta_{34}+180\eta_{56})\\ &\quad+(-108\eta_{012}-288\eta_{34})r_1^{2}\big],\\ \alpha_3 &= 1/2(r\partial_r\alpha_2+\alpha_1)\\ &= 2/3\,\xi^{-1}\big[(-128\eta_{56}-38\eta_{789})r_1^{-5}\\ &\quad+(80\eta_{34}+38\eta_{56}+38\eta_{789})r_1^{-3}\\ &\quad+(48\eta_{012}+48\eta_{34}+90\eta_{56})\\ &\quad+(-48\eta_{012}-128\eta_{34})r_1^{2}\big].\end{aligned}\tag{a29[4,5]}$$

3: tidal heating distribution, total heating

As seen in (a27) and (a4), both the stress and the equilibrium strain depend on r' and S (the angle between the line to the planet and the line to the point of evaluation). At a given fixed point in the satellite, r' and S change over time due to the planet's orbital motion and the satellite's rotation, so the stress and strain vary, too. Dissipation occurs due to the anelastic flexation of the satellite, which is equivalent to a phase delay applied to the elastic deformation. We denote the phase-delayed strain as e_{*ij}. The rate of energy dissipation per unit volume is

$$\begin{aligned}\dot W &= X_{ij}\dot e^*_{ij} = -p\delta_{ij}\dot e^*_{ij}+2\mu e_{ij}\dot e^*_{ij}\\ &= -p\partial_t(\nabla\cdot\vec u_*)+2\mu e_{ij}\dot e^*_{ij}\\ &= 2\mu e_{ij}\dot e^*_{ij},\end{aligned}\tag{a30}$$

where the summation convention is used. The incompressible assumption is used. In spherical coordinates, substitution of (a27) into (a30) gives:

$$\begin{aligned}\dot W = 2\mu R^2 g^{-2}k_2^2\\ &\times\big[A\dot A^*\alpha_0^2+2A\dot A^*\alpha_1^2\\ &+\big(A\dot B^*+B\dot A^*+A\dot C^*+C\dot A^*\big)\alpha_1\alpha_2\\ &+\big(B\dot B^*+C\dot C^*+2E\dot E^*\big)\alpha_2^2\\ &+2\big(D\dot D^*+H\dot H^*\big)\alpha_3^2\big].\end{aligned}\tag{a31}$$

Now we can see the separation of W's dependence on radius and on the angles. The r-dependence is completely expressed in α_i, and the θ- and ϕ-dependences are expressed in $A\dot A^*$, $A\dot B^*$ ... A, B... functions are determined by the planet's distance and orientation relative to the satellite, and $\dot A^*$, $\dot B^*$... are determined by the planet's orbital motion, the satellite's rotation, and the phase lags in the satellite's tidal responses.

We take $A\dot A^*$ as an example to study the form of the angle-dependent part of W: Let $(\theta',\ \phi')$, $(\theta,\ \phi)$ denote the colatitude and longitude of the planet and the point of evaluation. ϕ' and ϕ are measured from a particular meridian of the satellite, which is an instantaneous inertia frame of reference (χ_1). According to the spherical harmonic addition theorem,

$$\begin{aligned}A &= GMr'^{-3}\Sigma^2_{(m=0)}c_mP_{2m}\big(\cos\theta'\big)\\ &\quad\times P_{2m}(\cos\theta)\cos\big[m\big(\phi'-\phi\big)\big],\end{aligned}$$

where $c_m=(2-\delta_{0m})(2-m)!/(2+m)!$.

We then transform r', θ' and ϕ' to the planet's orbital elements to study the satellite's tidal response at different disturbing frequencies. Let Ω, ω, M, f, i, a denote the planet's longitude of ascending node, argument of pericenter, mean anomaly, true anomaly, inclination relative to the satellite's equatorial plane, and semi-major axis, respectively. Note that these elements are with respect to the inertia frame of reference (χ_0), so $\phi'=\Omega-\psi$, where ψ is the longitude of the basis meridian of χ_1 measured in χ_0.

The transform is based on

$$\begin{aligned}&P_{lm}\big(\cos\theta'\big)\cdot\begin{Bmatrix}\cos\\ \sin\end{Bmatrix}\big(m\phi'\big)\\ &=\Sigma^{l}_{(p=0)}F_{lmp}(i)\\ &\times\begin{Bmatrix}\cos\\ \sin\end{Bmatrix}[m(\Omega-\psi)+(l-2p)(\omega+f)+\kappa_{(l-m)}],\end{aligned}\tag{a32}$$

where $\kappa_x=\begin{cases}0, & x\text{ is even}\\ -\frac{\pi}{2}, & x\text{ is odd'}\end{cases}$

$$\begin{aligned}&F_{lmp}(i)=\\ &\sum_{t=0}^{\min\left[\frac{p}{\mathrm{floor}\left(\frac{l-m}{2}\right)}\right]}\frac{(2l-2t)!}{t!(l-t)!2^{2l-2t}}\sin^{l-m-2t}i\\ &\times\sum_{s=0}^{m}\binom{m}{s}\cos^s i\sum_{c=\max\left[\frac{0}{p-t-m+s}\right]}^{\min\left[\frac{l+s}{m+p+t}\right]-m-2t}\frac{\binom{l-m-2t+s}{c}\binom{m-s}{p-t-c}}{(l-m-2t)!}\\ &(-1)^{c-\mathrm{floor}\left(\frac{l-m}{2}\right)}\end{aligned}$$

(Kaula 1961), and the Hansen expansion

$$\left(\frac{R_{EM}}{a}\right)^m\begin{Bmatrix}\cos\\ \sin\end{Bmatrix}(nf)=\Sigma^{\infty}_{k=-\infty}X^{m,n}_k(e)\begin{Bmatrix}\cos\\ \sin\end{Bmatrix}(kM)\tag{a33}$$

So A(r', θ', ϕ', θ, ϕ) is transformed to:

$$\begin{aligned}A &= \Sigma^2_{m=0}\Sigma^2_{p=0}\Sigma^{\infty}_{q=-\infty}A_{2mpq},\\ A_{2mpq} &= GMa^{-3}\\ &\quad\times c_mP_{2m}(\cos\theta)F_{2mp}(i)G_{2pq}(e)\\ &\quad\times\cos\big[-m\phi-m\psi+\nu_{2mpq}+\kappa_m\big],\end{aligned}$$

where

$$\begin{aligned}\nu_{lmpq} &= m\Omega+(l-2p)\omega+(l-2p+q)M,\\ G_{lpq}(e) &= X^{-l-1,l-2p}_{(l-2p+q)}(e).\end{aligned}$$

Note that $\kappa_{(l-m)}\neq\kappa_m$ when l is 3, 5...

The phase delayed form is

$$\begin{aligned}A^*_{2mpq} &= GMa^{-3}\\ &\quad\times c_mP_{2m}(\cos\theta)F_{2mp}(i)G_{2pq}(e)\\ &\quad\times\cos\big[-m\phi-m\psi+\nu_{2mpq}+\kappa_m-\varepsilon_{2mpq}\big].\end{aligned}$$

The frequency of A^*_{lmpq} due to the orbital motion of the perturber and the rotation of the satellite is

$$\begin{aligned}f_{lmpq} &= -m\dot\psi+\dot\nu_{lmpq}\\ &= -m\dot\psi+m\dot\Omega+(l-2p)\dot\omega+(l-2p+q)\dot M.\end{aligned}$$

[4] When η=0, α_0 =8/3 -3r_1^2, α_3 =4/3 -4/3r_1^2.

[5] As a test, we compute values $k_2\cdot\alpha_i$ at particular parameter values, and compare the result with Peale & Cassen (1978) and Meyer *et al.* (2010). Take ρ=3.34, g=162, R=1.738e8, μ=6.5e11 (in cgs).
For η=0.5,
$k_2\cdot\alpha_0$=9.138e-3 r_1^{-5} -3.233e-2 r_1^{-3} +9.084e-2 -0.1135 r_1^2,
$k_2\cdot\alpha_1$=-2.284e-3r_1^{-5} +1.617e-2r_1^{-3} +9.084e-2 -3.784e-2r_1^2,
$k_2\cdot\alpha_2$=7.615e-4 r_1^{-5} +4.542e-2 -3.154e-2 r_1^2,
$k_2\cdot\alpha_3$=-3.046e-3r_1^{-5} +8.083e-3r_1^{-3} +4.542e-2 -5.046e-2r_1^2.
For η=0.95,
$k_2\cdot\alpha_0$=0.8874 r_1^{-5} -1.174 r_1^{-3} +0.7768 -0.8688 r_1^2,
$k_2\cdot\alpha_1$=−0.2219 r_1^{-5} +0.5871 r_1^{-3} +0.7768 -0.2896 r_1^2,
$k_2\cdot\alpha_2$=7.395e-2 r_1^{-5} +0.3884 -0.2413 r_1^2,
$k_2\cdot\alpha_3$=-0.2958 r_1^{-5} +0.2936 r_1^{-3} +0.3884 -0.3861 r_1^2.
These agree with $k_2'\cdot\alpha_0$, $k_2'\cdot\alpha_2$, $k_2'\cdot\alpha_1$, $k_2'\cdot\alpha_3$ in Peale & Cassen (1978) and Meyer *et al.* (2010), except for a typo and two errors in P&C 1978.

In completely damped 1:1 spin-orbit resonance, $\dot{\psi}=\dot{\Omega}+\dot{\omega}+\dot{M}$, so

$$f_{lmpq} = (l-2p-m)\dot{\omega} + (l-2p+q-m)\dot{M}.$$

When $\dot{\omega}/n$ is small, $f_{lmpq} \approx (l\text{-}2p+q\text{-}m)n$. So

$$\begin{aligned}
&A_{2mpq}\dot{A}^{*}_{2m'p'q'} \\
&= G^2M^2a^{-6}c_m c_{m'}P_{2m}(\cos\theta)P_{2m'}(\cos\theta) \\
&\quad\times F_{2mp}(i)F_{2m'p'}(i)G_{2pq}(e)G_{2p'q'}(e) \\
&\quad\times\left(-f_{2m'p'q'}\right) \\
&\quad\times\cos\left[-m\phi - m\psi + \nu_{2mpq} + \kappa_m\right] \\
&\quad\times\sin\left[-m'\phi - m'\psi + \nu_{2m'p'q'} + \kappa_{m'} - \varepsilon_{2m'p'q'}\right] \\
&= G^2M^2a^{-6}c_m c_{m'}P_{2m}(\cos\theta)P_{2m'}(\cos\theta) \\
&\quad\times F_{2mp}(i)F_{2m'p'}(i)G_{2pq}(e)G_{2p'q'}(e) \\
&\quad\times(-1)\left(2-2p'+q'-m'\right)n\cdot 1/2 \\
&\quad\times\Big\{\sin\left[-\left(m'+m\right)\phi - \left(m'+m\right)\psi\right. \\
&\quad\left.+\nu_{2m'p'q'} + \nu_{2mpq} + \kappa_{m'} + \kappa_m - \varepsilon_{2m'p'q'}\right] \\
&\quad+\sin\left[-\left(m'-m\right)\phi - \left(m'-m\right)\psi\right. \\
&\quad\left.+\nu_{2m'p'q'} - \nu_{2mpq} + \kappa_{m'} - \kappa_m - \varepsilon_{2m'p'q'}\right]\Big\}
\end{aligned} \tag{a34}$$

The secular terms are those with m+m' being even, and

$$\begin{aligned}
&2-2p-m = 2-2p'-m',\ q=q' \\
&\qquad(\text{i.e.}, f_{2mpq} = f_{2m'p'q'}),
\end{aligned}$$

or

$$\begin{aligned}
&2-2p-m = -\left(2-2p'-m'\right),\ q=-q' \\
&\qquad(\text{i.e.}, f_{2mpq} = -f_{2m'p'q'}).
\end{aligned}$$

Apply the form of phase lag in the constant-Q Darwin-Kaula tidal model

$$\varepsilon_{2mpq} = Q^{-1}\,\text{sign}(f_{2mpq}) \tag{a35}$$

to the expression, and ignore the periodic terms, we get the secular part of (a34):

$$\begin{aligned}
&A_{2mpq}\dot{A}*_{2m'p'q'} \\
&= G^2M^2a^{-6}c_m c_{m'}P_{2m}(\cos\theta)P_{2m'}(\cos\theta) \\
&\quad\times F_{2mp}(i)F_{2m'p'}(i)G_{2pq}(e)G_{2p'q'}(e) \\
&\quad\times 1/2\left(2-2p'+q'-m'\right)nQ^{-1}\,\text{sign}(2-2p'+q'-m') \\
&\quad\times\begin{cases}
\cos\left(m-m'\right)\phi \\
\left(m+m'\ \text{even},\ f_{2mpq}=f_{2m'p'q'}\right) \\
(-1)^m\cos\left(m+m'\right)\phi \\
\left(m+m'\ even,\ f_{2mpq}=-f_{2m'p'q'}\right) \\
0 \\
(\text{else})
\end{cases}
\end{aligned} \tag{a36}$$

The angle-averaged value is

$$\begin{aligned}
&A\dot{A}^{*}_{\theta\phi-\text{avg}} \\
&\quad= (4\pi)^{-1}\int_{[0,2\pi]}\int_{[0,\pi]} A\dot{A}^{*}\cdot\sin\theta\, d\theta\, d\phi \\
&\quad= G^2M^2a^{-6}nQ^{-1}\cdot 21/10\left(e^2+403/56e^4+\ldots\right).
\end{aligned} \tag{a37}$$

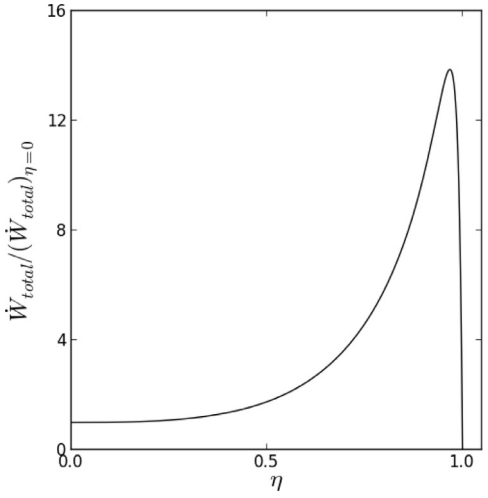

Fig. A.1. The dependence of W_{total} (scaled with $(W_{total})_{\eta=0}$) on η.

$A\dot{B}^{*}\ldots$, $A\dot{B}^{*}{}_{\theta\phi\text{-avg}}\ldots$ can be computed in a similar way. Then with (a31), we get the angle-averaged tidal heating:

$$\begin{aligned}
\dot{W}_{\theta\phi-\text{avg}} &= \mu G^2M^2nR^2a^{-6}Q^{-1}g^{-2}k_2^2 \\
&\quad\times\left(21/5\alpha_0^2 + 42/5\alpha_1^2\right. \\
&\quad-252/5\alpha_1\alpha_2 + 126\alpha_2^2 + \left.252/5\alpha_3^2\right) \\
&\quad\times\left(e^2+403/56e^4\right) + o\left(e^4\right).
\end{aligned} \tag{a38}$$

The total heating rate in the outer layer (up to e^2) is

$$\begin{aligned}
\dot{W}_{\text{total}} &= \int_{[R\cdot\eta,R]} 4\pi r^2\dot{W}_{\theta\phi-avg}dr \\
&= k_2^2\cdot 28\lambda/\xi\cdot 4\pi\mu G^2M^2nR^5e^2a^{-6}Q^{-1}g^{-2}.
\end{aligned} \tag{a39[6]}$$

Using parameters appropriate for Io[7], (a22) and (a39) give the relationship between $W_{\text{total}}/(W_{\text{total}})_{\eta=0}$ and η, as shown in Fig. A.1, which agrees well with Peale et al. (1979) and Meyer et al. (2010).

References

Beuthe, M., 2013. Spatial patterns of tidal heating. Icarus 223, 308–329. doi:10.1016/j.icarus.2012.11.020.

Cameron, A.G.W., Ward, W.R., 1976. the origin of the moon. Proc. Lunar Planet. Sci. Conf. 7, 120.

Canup, R.M., Asphaug, E., 2001. Origin of the moon in a giant impact near the end of the earth's formation. Nature 412, 708. doi:10.1038/35089010.

Canup, R.M., 2004. Simulations of a late lunar-forming impact. Icarus 168, 433. doi:10.1016/j.icarus.2003.09.028.

Canup, R.M., 2008. Lunar-forming collisions with pre-impact rotation. Icarus 196, 518. doi:10.1016/j.icarus.2008.03.011.

Canup, R.M., 2012. Forming a moon with an Earth-like composition via a giant impact. Science 338, 1052. doi:10.1126/science.1226073.

Cuk, M., Stewart, S.T., 2012. Making a moon from a fast-spinning Earth: a giant impact followed by resonance despinning. Science 338, 1047. doi:10.1126/science.1225542.

Elkins-Tanton, L., Burgess, S., Yin, Q.-Z., 2011. The lunar magma ocean: reconciling the solidification process with lunar petrology and geochronology. EPSL 304, 326. doi:10.1016/j.epsl.2011.02.004.

Hartmann, W.K., Davis, D.R., 1975. Satellite-sized planetesimals and lunar origin. Icarus 24. doi:10.1016/0019-1035(75)90070-6.

Huang, S., Petaev, M.I., Wang, W., Lock, J., Wu, Z., Stewart, S.T., Jacobsen, S.B., 2016. Lunar origin beyond the hot spin stability limit: stable isotopic fractionation. LPSC XXXVII..

Kaib, N., Cowan, N.B., 2015. The feeding zones of terrestrial planets and insights into moon formation. Icarus 252, 161–174. doi:10.1016/j.icarus.2015.12.042.

Kaula, W.M., 1961. Analysis of gravitational and geometric aspects of geodetic utilization of satellites. Geophy. J. Int. 5, 104–133. doi:10.1111/j.1365-246X.1961.tb00417.x.

[6] When η=0, we get λ=19, ξ=24, $W_{\text{total}} = k_2^2\cdot 133/6\cdot 4\pi\mu^E G^2M^2nR^5e^2a^{-6}Q^{-1}g^{-2}$.

[7] R=1.821e8, ρ=3.53, g=179.71, μ=6.5e11, in cgs.

Kaula, W.M., 1964. Tidal dissipation by solid friction and the resulting orbital evolution. Rev. Geophys. 2, 661–685. doi:10.1029/RG002i004p00661.
Lugmair, G.W., Shukolyukov, A., 1998. Early solar system timescales according to ^{53}Mn-^{53}Cr systematics. Geochim. Cosmochim. Acta 62, 2863. doi:10.1016/S0016-7037(98)00189-6.
Longhi, J., 2003. A new view of lunar ferroan anorthosites: postmagma ocean petrogenesis. J. Geophys. Res. 108, 1. doi:10.1029/2002JE001941.
Love, A.E.H., 1944. A Treatise on the Mathematical Theory of Elasticity, 4th Ed Dover publications, New York.
Mastrobuono-Battisti, A., Perets, H.B., Raymond, S.N., 2015. A primordial origin for the compositional similarity between the earth and the moon. Nature 520, 212. doi:10.1038/nature14333.
Meyer, J., Elkins-Tanton, L., Wisdom, J., 2010. Coupled thermal-orbital evolution of the early moon. Icarus 208, 1–10. doi:10.1016/j.icarus.2010.01.029.
Mignard, F., 1979. The evolution of the lunar orbit revisited. I. Moon Planets 20, 301–315. doi:10.1007/BF00907581.
Ojakangas, G.W., Stevenson, D.J., 1986. Episodic volcanism of tidally heated satellites with application to io. Icarus 66, 341. doi:10.1016/0019-1035(86)90163-6.
Pahlevan, K., Stevenson, D.J., 2007. Equilibration in the aftermath of the lunar-forming giant impact. EPSL 262, 438. doi:10.1016/j.epsl.2007.07.055.
Peale, S.J., Cassen, P., 1978. Contribution of tidal dissipation to lunar thermal history. Icarus 36, 245. doi:10.1016/0019-1035(78)90109-4.
Peale, S.J., Cassen, P., Reynolds, R.T., 1979. Melting of io by tidal dissipation. Science 203, 892–894. doi:10.1126/science.203.4383.892.
Reufer, A, Meier, M.M.M., Benz, W., Wieler, R., 2012. A hit-and-run giant impact scenario. Icarus 221, 296. doi:10.1016/j.icarus.2012.07.021.
Sussman, G.J., Wisdom, J., 2015. Structure and Interpretation of Classical Mechanics, second edition MIT Press ISBN:9780262028967.
Touboul, M., Klein, T., Bourdon, B., Palme, H., Weiler, R., 2007. Late formation and prolonged differentiation of the moon inferred from w isotopes in lunar metals. Nature 450, 1206. doi:10.1038/nature06428.
Touma, J., Wisdom, J., 1993. Lie–Poisson integrators for rigid body dynamics in the solar system. Astron. J. 107, 1189–1202. doi:10.1086/116931.
Turcotte, D.L., Schubert, G., 2002. Geodynamics. Cambridge University Press, Cambridge.
Wahr, J.M., Zuber, M.T., Smith, D.E., Lunine, J.I., 2006. Tides on Europa, and the thickness of europa's icy shell. J. Geophys. Res. 111, E12005. doi:10.1029/2006JE002729.
Wiechert, U., Halliday, A.N., Lee, D.-C., Snyder, G.A., Taylor, L.A., Rumble, D., 2001. Oxygen isotopes and the moon-forming giant impact. Science 294, 345. doi:10.1126/science.1063037.
Wieczorek, M.A., et al., 2013. The crust of the moon as seen by GRAIL. Science 339, 671–675. doi:10.1126/science.1231530.
Williams, J.G., Boggs, D.H., Ratcliff, J.T., 2005. Lunar fluid core and solid-body tides. LPSC XXXVI 1503.
Williams, J.G., et al., 2014. Lunar interior properties from the GRAIL million. JGR Planets 119, 1546–1578. doi:10.1002/2013JE004559.
Wisdom, J., Holman, M., 1991. Symplectic maps for the N-body problem. Astron. J. 102, 1528–1538. doi:10.1086/115978.
Wisdom, J., Tian, Z., 2015. Early evolution of the earth–moon system with a fast-spinning earth. Icarus 256, 138. doi:10.1016/j.icarus.2015.02.025.
Zahnle, K., Arndt, N., Cockell, C., Halliday, A., Nisbet, E., Selsis, F., Sleep, N.H., 2007. Emergence of a habitable planet. Space Sci. Rev. 129, 35–78. doi:10.1007/s11214-007-9225-z.
Zhang, J., Dauphas, N., Davis, A.M., Leya, I., Fedkin, A., 2012. The proto-Earth as a significant source of lunar material. Nat. Geosci. 5, 240. doi:10.1038/ngeo1429.